

Energy Level Alignment of Formamidinium Tin Iodide in Contact with Organic Hole Transport Materials

Jonas Horn and Derck Schlettwein*

Tin-based perovskites provide environmentally less problematic alternatives to established lead halide-based absorbers used in today's most efficient perovskite solar cells. However, tin-based cells still suffer from reduced power conversion efficiency and stability when compared to lead-based analogues. To facilitate the adoption of the very successful n-i-p cell geometry, efficient contact to hole transport materials (HTMs) is needed that can be deposited on top of the tin-based perovskite layer, ideally by physical vapor deposition to protect the underlying perovskite. As possible candidates for such HTMs, the growth and the interface formation of 4,4',4''-tris[phenyl(m-tolyl)amino]triphenylamine (m-MTDATA), pentacene, and copper phthalocyanine with formamidinium tin iodide by Kelvin probe force microscopy are systematically studied. For the contact to m-MTDATA, the formation of a Mott-Schottky junction is revealed, whereas an interfacial dipole is formed for the latter two. Doping densities within the organic semiconductor are determined and indicate ion migration from the perovskite.

major obstacle that prevents these materials from entering the market.^[8,9] A strategy often pursued to overcome this issue consists of the replacement of Pb by Sn, resulting in a material with similar structure and quite promising optoelectronic properties that should cause less problems to the environment at, however, the price of further reduced (ambient) stability and considerably lower efficiency in PSCs.^[10,11] Nevertheless, formamidinium tin iodide (FASnI₃) currently delivers the highest PCEs (>10%) among Pb-free perovskite-based solar cells using a p-i-n geometry with poly(3,4-ethylenedioxythiophene) polystyrene sulfonate or NiO_x as hole transport material (HTM) and C₆₀ or the indene-C₆₀ bisadduct as electron transport material (ETM).^[12–16] The (regular) n-i-p geometry, which had turned out more efficient for

1. Introduction


Hybrid organic-inorganic halide perovskites were intensely investigated during the last decade not only because of their potential as light-absorber materials in thin-film photovoltaics but also because of optoelectronic and semiconducting properties that make them interesting for other applications.^[1–4] Power conversion efficiencies (PCEs) in perovskite solar cells (PSCs) surpassing 25%^[5] impressively documented in a rich set of publications on this class of materials^[6] prove the potential. Aside from problems in long-term stability,^[7] the presence of toxic lead halides in all high-efficiency PSCs is regarded as a

lead-based devices, currently falls back in terms of efficiency when tin-based absorber layers are used not only because of inferior film quality for FASnI₃ deposited on TiO₂ but also because of poor energy-level-alignment with solution-processed HTMs, which have been tested so far.^[17]

In this work, contact formation of FASnI₃ to alternative organic HTMs was studied. To avoid potential problems arising from solution processing, the HTMs were vapor-deposited onto FASnI₃. Further, vapor deposition allows preparation of high-purity films, and additional organic solvents are not needed.^[18–20] Further, metallic back contacts are typically deposited via physical vapor deposition (PVD), which enables deposition of the final two layers without breaking the vacuum, leading to a minimum of environmental stress during cell preparation. As promising HTM candidates, 4,4',4''-tris[phenyl(m-tolyl)amino]triphenylamine (m-MTDATA), copper phthalocyanine (CuPc), and pentacene were studied (**Figure 1**). These materials were chosen because they already have been established as contact for MAPbI₃ (CuPc^[20,21]), are archetypal for the class of vapor-deposited organic semiconductors (pentacene^[22]), or promise a good match with the valence band (VB) of FASnI₃ (m-MTDATA,^[23,24] which is fairly well established in the context of organic light-emitting diodes). All three materials can be doped by co-evaporation of an acceptor molecule (e.g., tetrafluoro-tetracyano-quinodimethane (F₄-TCNQ) for m-MTDATA^[25,26] and CuPc^[27] or 2,2'-(perdiylidene)dimalononitrile (F₆-TCNNQ) for pentacene^[28]), which leads to an increase in conductivity allowing their application as HTMs in technical thin-film devices. Further, these three offer strongly differing structure in thin films: while m-MTDATA forms an organic glass in an amorphous

J. Horn, D. Schlettwein
Institute of Applied Physics
Justus Liebig University Giessen
Heinrich-Buff-Ring 16, 35392 Giessen, Germany
E-mail: schlettwein@uni-giessen.de

J. Horn, D. Schlettwein
Center for Materials Research (ZfM)
Justus Liebig University Giessen
Heinrich-Buff-Ring 16, 35392 Giessen, Germany

 The ORCID identification number(s) for the author(s) of this article can be found under <https://doi.org/10.1002/pssa.202100698>.

© 2022 The Authors. physica status solidi (a) applications and materials science published by Wiley-VCH GmbH. This is an open access article under the terms of the Creative Commons Attribution-NonCommercial-NoDerivs License, which permits use and distribution in any medium, provided the original work is properly cited, the use is non-commercial and no modifications or adaptations are made.

DOI: 10.1002/pssa.202100698

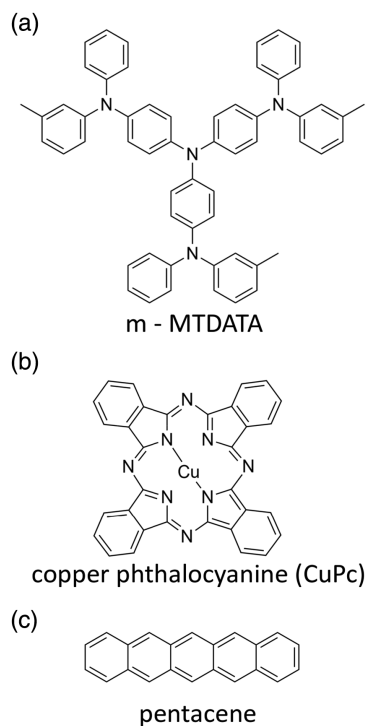


Figure 1. Organic molecules investigated as possible HTM. a) m-MTDATA, b) CuPc, and c) pentacene.

structure,^[29] CuPc builds polycrystalline layers^[30,31] and pentacene preferentially grows in large islands of high crystal quality.^[32] We focus on the alignment of energy levels at the interface as a central property to allow a low contact resistance, low rate of interfacial recombination, and hence optimum harvest of the built-in voltage by charge extraction at the interface.^[33] Previous studies on FASnI₃-based PSCs showed the relevance of the energy level alignment of the absorber with ETM and HTM and proved that careful optimization can improve the solar cell properties.^[34–36] Kelvin probe force microscopy (KPFM) is used to measure the contact potential difference (CPD) between the probe and the sample surface at high local resolution, which allows to calculate the work function (Φ) of the surface upon stepwise deposition of HTMs via PVD on top of FASnI₃ to monitor contact formation upon increasing HTM thickness. KPFM was previously applied to lead- and tin-based perovskites and PSCs to understand, e.g., the potential drop throughout a PSC or the formation of local charges and mobility of ions within the perovskite layer.^[18,37,38]

2. Results

Morphology and the work function Φ of each FASnI₃ layer were investigated by KPFM to provide widely identical starting conditions for subsequent HTM deposition and characterization. Independent of the substrate (TiO₂, ITO), the morphology of the FASnI₃ films was widely constant with a similar distribution of apparent grain size (diameter of about 200–800 nm) and root mean square roughness values (36 ± 9 nm) as also confirmed by

scanning electron microscopy (SEM) (Figure S1, Supporting Information). $\Phi = 4.39 \pm 0.037$ eV was obtained for the pristine perovskite layers which are closer to the conduction band minimum (3.9–4.1 eV, measured by inverse photoelectron spectroscopy^[36,39]) than to the valence band maximum (5.3 eV, obtained by ultraviolet photoelectron spectroscopy (UPS)^[36]). Slight n-type doping of the perovskite films is thereby indicated. P-type doping of FASnI₃, which has often been reported, is usually explained by undesired and often detrimental oxidation of Sn(II) to Sn(IV) or by the presence of Sn(IV) in the starting materials. This is not observed in the present case, speaking in favor of successful suppression of such chemical degradation. N-type conduction, as in the present case, was reported earlier if the process of oxidative self-doping was actively suppressed.^[40] Further, an almost constant value of Φ (± 0.037 eV only) for 16 samples speaks in favor of a highly reproducible preparation process for the perovskite layers and well-suited starting conditions for the investigation of the contact formation. For measurements related to CuPc, however, we found an influence of the morphology on the measured work function (cross talk) leading to artifacts of a reduced Φ at FASnI₃ grain boundaries, as discussed later.

To study film growth and the change of Φ induced by the contact material, different HTMs were stepwise deposited on top of the perovskite and were intermittently studied by AFM and KPFM. The morphology of the thin films with increasing thickness of the organic HTMs on FASnI₃ is presented in **Figure 2** and varies substantially among the investigated HTMs. At an average thickness d of 2 nm, m-MTDATA (top row) grows in spherical islands of about 8–10 nm in height and diameter that cover an area of approximately one quarter of the FASnI₃ surface only. An immediate shift of Φ (**Figure 3**), however, indicates the presence of a monolayer of m-MTDATA in addition to the islands observed in the morphology. For an average thickness above 30 nm, the islands form a continuous film, however, still with visible grain boundaries. For even larger average thickness, the grain boundaries became less defined and the surface roughness was reduced. Similar film growth of m-MTDATA was reported on bare ITO substrates.^[41] The growth of CuPc (**Figure 2**, center) starts in a similar growth mode ($d = 3$ nm) with, however, a strongly increased concentration of homogeneously distributed crystallization seeds and, therefore, forms smaller islands. Consequently, the layer of CuPc already covers the underlying perovskite at a lower d of around 15 nm. The morphology of the CuPc film remains largely unchanged even for higher average thickness, which is independently confirmed by SEM analysis (**Figure S2**, Supporting Information). This growth of CuPc is widely comparable to other reports on vapor-deposited thin films of CuPc deposited at room temperature.^[30,42,43] Pentacene (**Figure 2**, bottom row) differs in its growth mode, as it shows large flat islands already for the smallest d . Due to the small height difference, these islands (≈ 3 nm) are barely detected in the morphology images, but give a clear contrast in the frequency shift (**Figure S3**, Supporting Information). Based on the height of these islands of around 3 nm, we can assume the formation of the well-known thin-film phase with an in-plane spacing of around 1.5 nm.^[44,45] Such growth mode can be explained by either high mobility of pentacene on the perovskite surface or the establishment of a pentacene monolayer followed by diffusion of pentacene on this

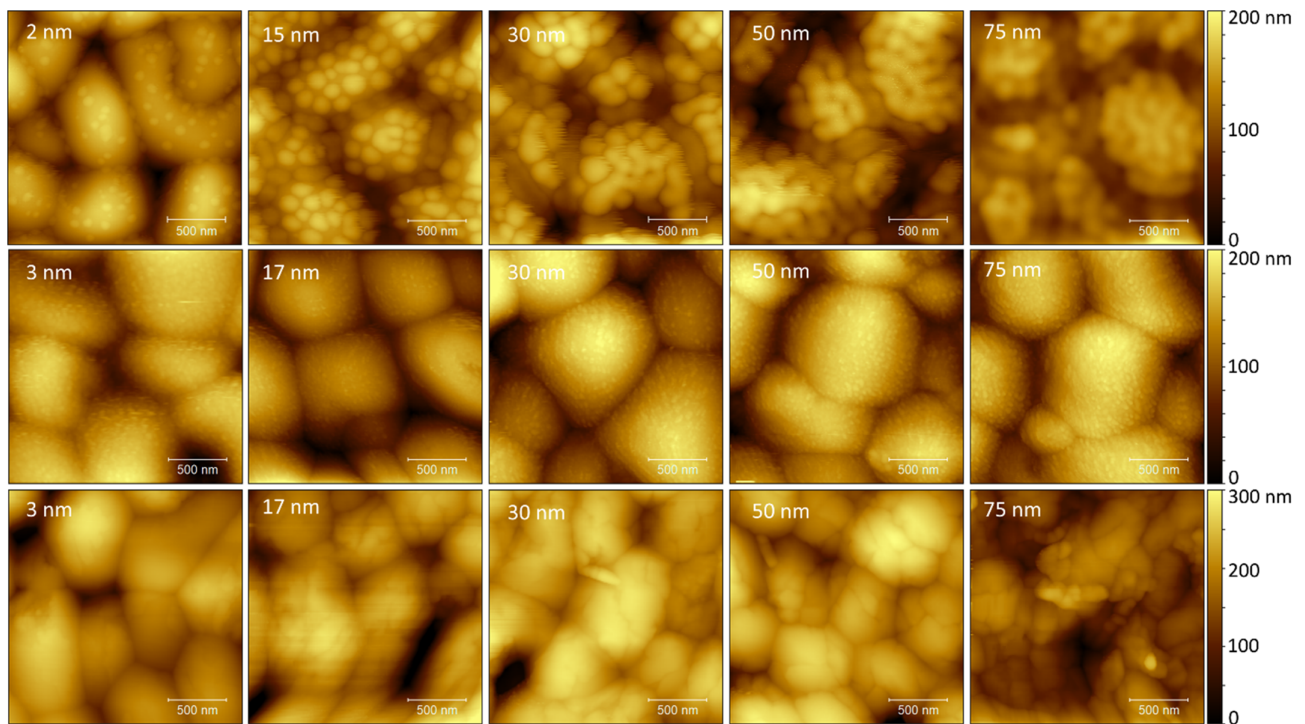


Figure 2. Sample morphology for different average film thickness d of the organic layer m-MTDATA (top row), CuPc (center), and pentacene (bottom row) on top of FASnI₃.

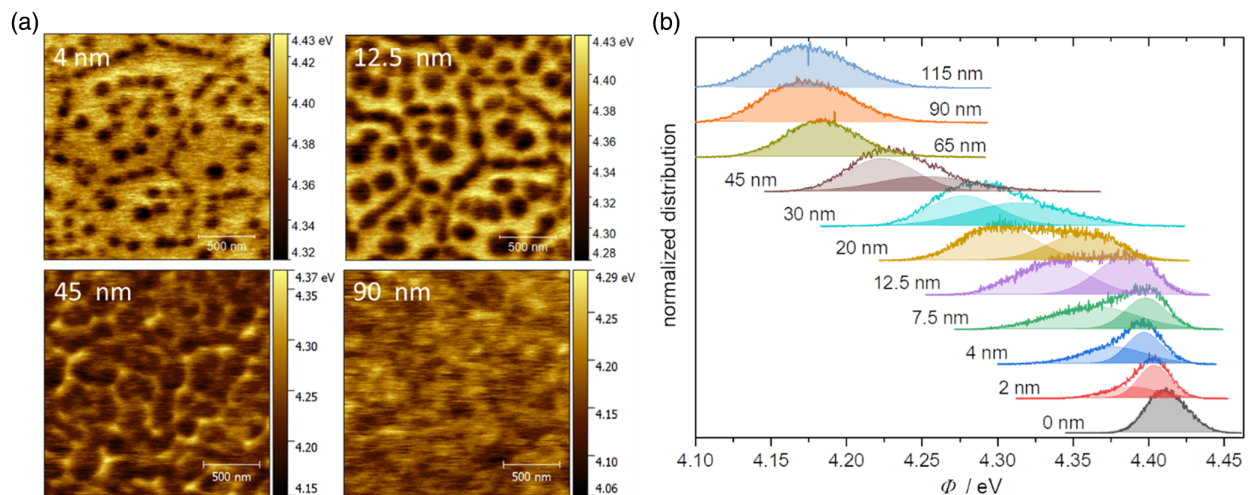


Figure 3. a) Work function of 4, 12.5, 45, and 90 nm of m-MTDATA deposited on FASnI₃. b) Distribution of work function Φ depending on average thickness d of m-MTDATA deposited onto FASnI₃ and corresponding Gaussian fits with one (0, 65, and 90 nm) or two (2, 4, 7.5, 12.5, 20, 30, and 45 nm) contributions.

monolayer with low activation energy. Either way, a closed layer of pentacene is reached already for a rather small d of 15 nm. From the morphological point of view, all three investigated materials are well suited as HTMs, as they form closed layers at reasonable $d \approx 30$ nm, sufficiently thin to allow fast hole transport through the layer toward the back electrode, given sufficiently high hole mobility^[46,47] in combination with appropriate doping to increase the charge carrier concentration.^[25,27,28]

When m-MTDATA is used, one should consider the deposition of at least 50 nm to safely avoid shunt formation and thereby increased interfacial recombination.

The contact potential difference of the deposited films was measured simultaneously to the morphology. Thereby, the local distribution of Φ was obtained as shown in Figure 3a for 4, 12.5, 45, and 90 nm m-MTDATA on FASnI₃. Areas of a reduced Φ for $d = 4$ and 12.5 nm can be clearly correlated to islands of m-MTDATA grains

(Figure S4, Supporting Information) surrounded by regions of higher Φ dominated by either pristine FASnI₃ or a thin layer of m-MTDATA on FASnI₃. The contributions of the low and high work function signals are quite similar for $d = 4$ and 12.5 nm average thickness, indicating that about half the area of FASnI₃ is covered by MTDATA in this thickness regime. For $d = 45$ nm, areas of higher Φ are barely seen and disappear for $d = 90$ nm, well in line with a morphology of a thick uniform shell of m-MTDATA on FASnI₃. Complete coverage of FASnI₃ with m-MTDATA is proven, as we detect only one uniform work function assigned to this shell of m-MTDATA. By analyzing the shape and position of the distribution of Φ (Figure 3b), we find a systematic decrease of the average of Φ with increasing d of m-MTDATA, which saturates at $d \approx 90$ nm. The shape of the distribution changes from a single Gaussian (bare FASnI₃) to a convolution of two Gaussians (4–45 nm, islands of m-MTDATA surrounded by regions of higher Φ) and back to a single Gaussian for a closed shell of m-MTDATA (65–115 nm). Φ_1 and Φ_2 resulting from Gaussian fits for m-MTDATA are summarized in Figure S5, Supporting Information. When assuming a Volmer–Weber-type growth with separated islands surrounded by bare FASnI₃, we would expect the high work function part (Φ_2) to always match the perovskite work function. As Φ_2 is slightly decreased compared to the perovskite work function, but stays constant from 4 to 12.5 nm, we infer that a uniform thin layer of m-MTDATA (Φ_2) is covering the perovskite surface before the growth of islands dominates (Stranski–Krastanov growth). The work function of these islands (Φ_1) decreases with increasing d , while Φ_2 of the thin layer remains almost constant until $d \approx 15$ nm (Figure S5, Supporting Information). Preferential growth of the islands at a widely constant thickness of the thin layer is thereby indicated, which is confirmed by the morphology (Figure S4, Supporting Information). For intermediate d of m-MTDATA (20–45 nm), the intensity ratio $\Phi_1:\Phi_2$ is decreasing, confirming that the islands of m-MTDATA are covering increasing parts of the surface. Further, Φ_2 is also decreasing, which indicates that the layer between islands is also growing in thickness to finally form a uniform closed shell (65–115 nm).

The corresponding analysis of Φ intermittent to the deposition of CuPc (Figure S6, Supporting Information) shows that the distribution for most average film thicknesses (including the measurement of bare perovskite without CuPc) consists of two Gaussian contributions with increased full width at half maximum (FWHM), which we assign to cross talk artifacts induced by the surface morphology, as can be seen by reduced work function at grain boundaries of the perovskite and increased work function in the center of the grains resulting from tip inhomogeneities presumably originating from the sticking of CuPc at the AFM tip during earlier scans (Figure S7, Supporting Information) as this effect was observed for CuPc only. The distribution of Φ gets broader and shifts toward lower Φ with increasing d . Consequences of contact formation between the n-type perovskite and the p-type CuPc were clearly observed (Figure 4) and were similar to those established for m-MTDATA. In the detailed analysis of Φ as a function of film thickness for pentacene (Figure S8, Supporting Information), it was confirmed that closed layers were already reached at least for $d \approx 15$ nm, corresponding to a good fit by only one Gaussian in the distribution. For an average thickness below this limit, we

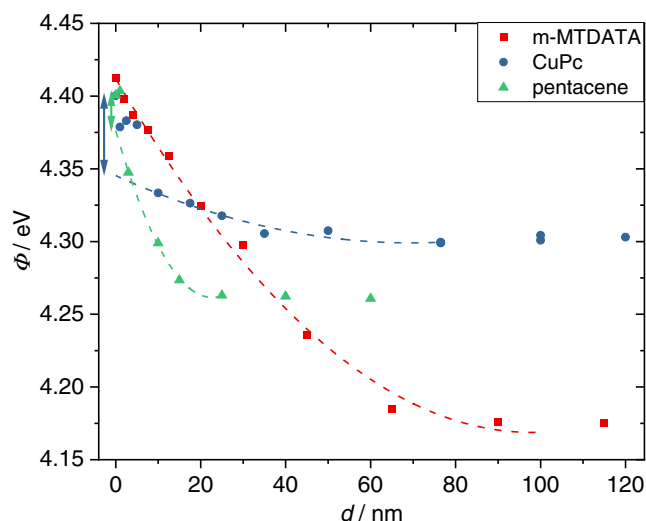


Figure 4. Average of the work function Φ as a function of average film thickness d of the organic HTM m-MTDATA, CuPc, and pentacene. The dashed lines represent fits using Equation (1). The energy differences Δ caused by the interfacial dipoles that resulted for CuPc and pentacene are marked by arrows at 0 nm.

find additional contributions which can be related to the work function of the uncovered perovskite (1 nm, 3 nm), but also to a variation in height of the pentacene islands, significant for thin films ($d = 5$ and 10 nm). A decreasing work function for increasing film thickness as a consequence of contact formation was observed for pentacene as well (Figure 4 and Figure S8, Supporting Information).

With increasing d , Φ was found to decrease for all three HTMs (Figure 4). This was expected as the bulk value of Φ of all three materials is lower than that of FASnI₃. The slope of decrease and the value at which the decrease was completed, however, differed. When m-MTDATA was deposited, a monotonous decrease was observed for $d < 100$ nm, where Φ finally saturated at $\Phi_{\text{m-MTDATA}} = 4.17$ eV. For CuPc, Φ saturated at $d \approx 60$ nm and $\Phi_{\text{CuPc}} = 4.3$ eV. Pentacene led to a stronger and steeper decrease and saturated at $d \approx 30$ nm and $\Phi_{\text{pentacene}} = 4.26$ eV. Dependent on the growth mode established for each HTM on FASnI₃, the average film thickness needed for a saturation of the work function differed significantly among the three materials $d_{\text{m-MTDATA}} > d_{\text{CuPc}} > d_{\text{pentacene}}$. The saturated values of Φ can be interpreted as work function characteristic for the bulk of the HTMs. The presently observed values, however, differ from reported work functions obtained by UPS in all three cases (pentacene: 3.9–4.1^[48,49] eV, CuPc: 3.7–3.8 eV,^[50,51] and m-MTDATA: 4.3 eV^[52,53]). This difference can be explained either by the different techniques used to obtain these values (photoelectron spectroscopy versus KPFM) or by differences in equilibration with the substrate. Different electronic coupling, charge transfer, or even ion migration from the semiconducting perovskite into the deposited organic layer, as it was reported for the interface between FASnI₃ with C₆₀,^[36] could cause such a difference.

For the interface with an organic semiconductor, the formation of an interfacial dipole (Fermi level pinning) as a possible consequence of such local interfacial charge transfer is not

expected if the Fermi energy of the underlying substrate is well above the highest occupied molecular orbital (HOMO) level of the organic.^[52] which is the case for all three investigated HTMs on FASnI₃. However, the decrease of Φ with increasing d for pentacene and CuPc shows a clear step below $d = 10$ nm, speaking in favor of dipole formation by the transfer of negative charge (e^- or I^- from FASnI₃ to pentacene and CuPc). On the contrary, the decrease of Φ during deposition of m-MTDATA proceeds in a monotonous way, with no indication of any interfacial dipole. When assuming constant charge density within a space charge layer (Schottky approximation), one would expect a parabolic dependence of the potential (and thus the work function Φ) within the space charge layer

$$\Phi(d) = \Phi_{\text{OSC}} - \frac{qN_d}{2\epsilon_r\epsilon_0} (d - d_{\text{SCL}})^2 \quad (1)$$

with Φ_{OSC} as the saturation value of the work function, N_d as dopant density, ϵ_r as relative permittivity of the organic material (m-MTDATA: 2.7,^[54] CuPc: 3.6,^[55] pentacene: 3.9^[56]) and d_{SCL} as the width of the space charge layer.^[57,58] Fit results of the experimental data (Figure 4) are summarized in **Table 1**. For m-MTDATA, the full dataset was well described by Equation (1), whereas an interfacial dipole was detected for CuPc and pentacene as the data below $d = 5$ nm (CuPc) and $d = 3$ nm (pentacene) had to be excluded from the fit. The energy difference Δ caused by this interfacial dipole is estimated by the difference between Φ (0 nm) and the corresponding value of the fit function. Despite the fact that the formation of interfacial dipoles by organic molecules is difficult to predict on a molecular level and detailed experiments are typically needed for each individual

Table 1. Fit results obtained by fitting the data in Figure 4 according to Equation (1).

Organic semiconductor	Φ_{OSC} [eV]	d_{SCL} [nm]	N_d [10^{15} cm^{-3}]	c [ppm]	Δ [meV]
m-MTDATA	4.17 ± 0.004	98 ± 3.5	7.6 ± 0.6	8.4 ± 0.7	0
CuPc	4.3 ± 0.002	70 ± 6.8	3.7 ± 1	2.2 ± 0.6	55
Pentacene	4.26 ± 0.001	22.7 ± 0.7	98 ± 7.7	34 ± 2.7	24

combination of materials,^[59–62] one is tempted to correlate Δ with a permanent dipole moment. This was discussed earlier for self-assembled monolayers of small molecules on methylammonium lead iodide.^[63] As opposed to CuPc and pentacene, we calculated a permanent dipole moment for m-MTDATA (Table S1, Supporting Information). One may speculate that atomic rearrangement during interface formation and subsequent appropriate arrangement of the permanent dipole of m-MTDATA compensates for possible interfacial dipoles, whereas this would not be possible for CuPc or pentacene.

The values obtained for N_d in the space charge region correspond to doping concentrations c (Table 1) of about one acceptor for each 10^5 – 10^6 molecule. This is less than, e.g., that found in intentionally doped pentacene, but significantly more than that found in pristine pentacene films.^[64] Such doping most likely stems from halogen migration into the organic HTMs from the interface with the perovskite. Halogen ions are known to be highly mobile within the perovskite layer.^[65,66] Also for conjugated molecular organic thin films, a mobility of halogen molecules and halide ions was reported (CuPc,^[67] pentacene,^[68] m-MTDATA^[69]).

The measured change of Φ is directly translated into shifts of the HOMO and the lowest unoccupied molecular orbital (LUMO) levels as shown in the energy-level diagram of **Figure 5**. The comparison of the three HTMs shows a driving force for hole injection from the VB of FASnI₃ to the HOMO of the HTM that is larger for pentacene or CuPc compared to m-MTDATA. For all three investigated contacts, hole accumulation can be assumed as a consequence of the band bending, similar to the reported contact formation of CuPc with the lead-based perovskite CH₃NH₃PbI₃.^[50] The electron blocking characteristics, however, are assured by a sufficiently high energy barrier between the conduction band (CB) of FASnI₃ and LUMO of the organic semiconductor in all three cases. The energy difference caused by the interfacial dipole of FASnI₃/CuPc is of a similar size as the overall band bending, while that of FASnI₃/pentacene is considerably smaller. In both cases, effective hole transfer from the perovskite into the HTM is not blocked by the dipole formation.

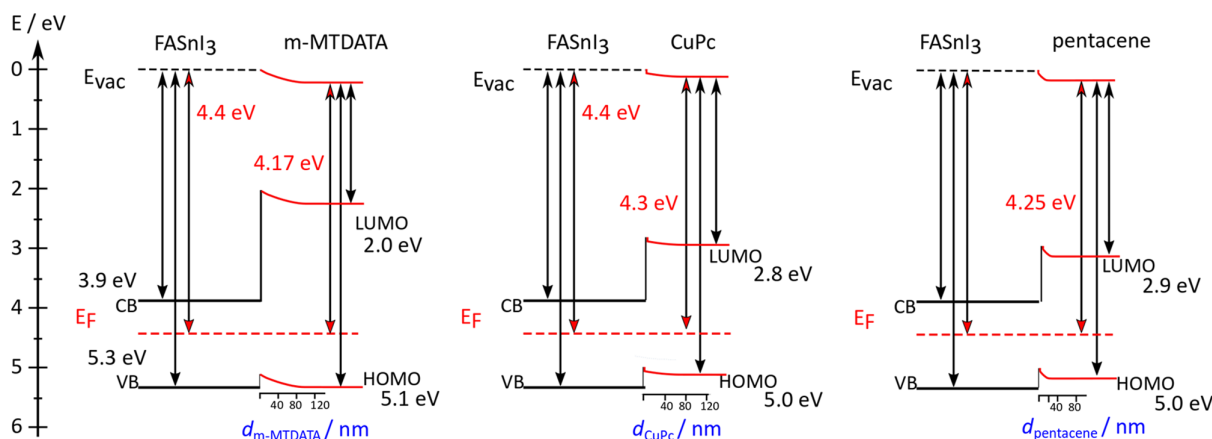


Figure 5. Contact formation constructed using thickness-dependent Φ (red numbers) of m-MTDATA, CuPc, and pentacene deposited on FASnI₃ in combination with literature values (black numbers).^[31,42,43,46]

3. Conclusions

The contacts of FASnI₃ with m-MTDATA, CuPc, and pentacene fulfill the fundamental prerequisite of an appropriate energy level alignment to be used as vapor-deposited HTMs in tin-based PSCs. Thin films with an average film thickness of about 30 nm only were shown to uniformly cover FASnI₃ opening options to avoid both shunt formation and high series resistance in prospective cells. An interfacial dipole that, however, is not expected to negatively affect the hole transfer from FASnI₃ was formed for CuPc and pentacene, but not for m-MTDATA. The observed band bending in the contacts was fitted based on the Schottky approximation and indicated ion migration from the underlying perovskite layer to all three of the investigated HTMs. To implement the investigated materials in PSCs, additional doping of the organic semiconductor layer, e.g., by co-evaporation will be required to achieve sufficiently high conductivity and thus allow facile hole transport as reported for CuPc in lead-based PSCs.^[70]

4. Experimental Section

Sample Preparation: Fluorine-doped tin oxide (FTO, Zhuhai Kaivo Optoelectronic Technology Co., Ltd.) was cleaned by subsequent ultrasonication for 10 min with an aqueous detergent (RBS solution, Roth), n-propanol (Roth), and acetone (Roth). After 10 min of UV-ozone cleaning, a thin layer of TiO₂ was deposited onto the FTO substrates by spin-coating a commercial solution (Ti-Nanoxide BL/SC, Solaronix) at 4000 rpm for 30 s followed by annealing in air at 500 °C for 60 min resulting in a 65 nm thick layer of TiO₂ as measured by SEM cross section. After an additional UV-ozone treatment, the samples were transferred into a glovebox filled with nitrogen (<1 ppm H₂O, <1 ppm O₂). A 1 M solution of SnI₂ (Sigma-Aldrich, 99.999 %), CH(NH₂)₂I (FAI, Greatcell Solar), and 0.1 M SnF₂ (Alfa Aesar, 99%) dissolved in a mixture of dimethylformamide (Acros) and dimethylsulfoxide (Acros) (v:v, 4:1) was used as a precursor for perovskite deposition. The thin layer of FASnI₃ was prepared by spin-coating at 4000 rpm for 60 s while applying chlorobenzene (Acros) as anti-solvent 12 s before the end of the rotation. After spin-coating, the samples were heated at 65 °C for 30 s and at 100 °C for 30 min. The thin film of FASnI₃ consists of large grains in the range of hundreds of nanometers with an overall thickness of around 265 nm, as measured by SEM cross section. To minimize sample degradation, the average storage time of the FASnI₃ films was minimized and kept below 24 h in every case. To avoid degradation of the perovskite layer, the samples were transferred without any contact to an ambient environment into a vacuum chamber containing an atomic force microscope (AFM; Vacuscope 1000 AIST-NT) as well as a physical vapor deposition system. Organic hole transport layers m-MTDATA (Sigma-Aldrich, 98%), pentacene (Sigma-Aldrich, 99.9%), and CuPc (Sigma-Aldrich, 99.99%) were vapor-deposited from resistively heated boron nitride crucibles while controlling the deposition rate with a calibrated quartz microbalance. The integrated signal served to determine the average film thickness *d*. The deposition rates were kept between 0.3 and 0.5 nm min⁻¹ in every case. Film morphology appeared not to be affected by variation of the deposition rate within this range.

Measurements: Before and intermittent to deposition, the morphology was measured in noncontact mode AFM and the contact potential difference between the conductive tip and the sample surface was analyzed by KPFM. The work function Φ was calculated by referencing to Φ of a freshly cleaved highly oriented pyrolytic graphite (HOPG, ZYA quality, MikroMasch) before and after each measurement ensuring a constant Φ of the tip during a measurement. Φ of HOPG had been established by various techniques as 4.6 eV.^[71,72] Frequency-modulated Kelvin probe force microscopy (FM-KPFM) was performed in a two-pass technique to obtain the morphology in a first scan and the contact potential difference

in a second scan, lifted above the film surface to minimize morphological cross talk. The contact potential between the gold-coated tip (OPUS 160AC-GG, radius <30 nm) and a given surface was obtained by applying an AC voltage (2 V at 1 kHz) to modulate the mechanical vibration of the cantilever at its first resonance frequency. The local resolution of the CPD can be assumed equal to the tip apex, which was reported to be around 50 nm^[73] and this was confirmed in the present setup.^[18] The occurrence of different values of Φ in each measured image was determined by Gwyddion 2.55 and plotted as a histogram which was fitted using Gaussian functions.

Supporting Information

Supporting Information is available from the Wiley Online Library or from the author.

Acknowledgements

The authors acknowledge the financial support from the Deutsche Forschungsgemeinschaft (DFG) within the projects SCHL 340/21-3 and RTG 2240.

Open access funding enabled and organized by Projekt DEAL.

Conflict of Interests

The authors declare no conflict of interest.

Data Availability Statement

The data that support the findings of this study are available from the corresponding author upon reasonable request.

Keywords

contact formation, KPFM, lead-free perovskites, organic semiconductors, photovoltaics, PVD

Received: October 13, 2021

Revised: November 29, 2021

Published online: January 17, 2022

- [1] D. B. Mitzi, C. A. Feild, W. T. A. Harrison, A. M. Guloy, *Nature* **1994**, 369, 467.
- [2] A. Kojima, K. Teshima, Y. Shirai, T. Miyasaka, *J. Am. Chem. Soc.* **2009**, 131, 6050.
- [3] C. R. Kagan, *Science* **1999**, 286, 945.
- [4] G. C. Papavassiliou, *Mol. Cryst. Liq. Cryst. Sci. Technol. Sect. A* **1996**, 286, 231.
- [5] M. Green, E. Dunlop, J. Hohl-Ebinger, M. Yoshita, N. Kopidakis, X. Hao, *Prog. Photovoltaics Res. Appl.* **2021**, 29, 3.
- [6] A. K. Jena, A. Kulkarni, T. Miyasaka, *Chem. Rev.* **2019**, 119, 3036.
- [7] N. Li, X. Niu, Q. Chen, H. Zhou, *Chem. Soc. Rev.* **2020**, 49, 8235.
- [8] S. A. U. Hasan, D. S. Lee, S. H. Im, K.-H. Hong, *Sol. RRL* **2019**, 131, 1900310.
- [9] S. Maranghi, M. L. Parisi, R. Basosi, A. Sinicropi, *Open Res. Eur.* **2021**, 1, 44.
- [10] N. K. Noel, S. D. Stranks, A. Abate, C. Wehrenfennig, S. Guarnera, A.-A. Haghhighirad, A. Sadhanala, G. E. Eperon, S. K. Pathak, M. B. Johnston, A. Petrozza, L. M. Herz, H. J. Snaith, *Energy Environ. Sci.* **2014**, 7, 3061.

- [11] A. Aftab, M. I. Ahmad, *Sol. Energy* **2021**, 216, 26.
- [12] K. Nishimura, M. A. Kamarudin, D. Hirotoni, K. Hamada, Q. Shen, S. Iikubo, T. Minemoto, K. Yoshino, S. Hayase, *Nano Energy* **2020**, 74, 104858.
- [13] T. Nakamura, T. Handa, R. Murdey, Y. Kanemitsu, A. Wakamiya, *ACS Appl. Electron. Mater.* **2020**, 2, 3794.
- [14] T. Wang, F. Zheng, G. Tang, J. Cao, P. You, J. Zhao, F. Yan, *Adv. Sci.* **2021**, 11, 2004315.
- [15] X. Jiang, F. Wang, Q. Wei, H. Li, Y. Shang, W. Zhou, C. Wang, P. Cheng, Q. Chen, L. Chen, Z. Ning, *Nat. Commun.* **2020**, 11, 1245.
- [16] E. Jocar, P.-Y. Cheng, C.-Y. Lin, S. Narra, S. Shahbazi, E. Wei-Guang Diao, *ACS Energy Lett.* **2021**, 6, 485.
- [17] N. Sun, W. Gao, H. Dong, Y. Liu, X. Liu, Z. Wu, L. Song, C. Ran, Y. Chen, *ACS Energy Lett.* **2021**, 6, 2863.
- [18] J. Horn, D. Schlettwein, *J. Mater. Res.* **2020**, 35, 2897.
- [19] M. Urbani, G. de La Torre, M. K. Nazeeruddin, T. Torres, *Chem. Soc. Rev.* **2019**, 48, 2738.
- [20] W. Ke, D. Zhao, C. R. Grice, A. J. Cimaroli, G. Fang, Y. Yan, *J. Mater. Chem. A* **2015**, 3, 23888.
- [21] T. Duong, J. Peng, D. Walter, J. Xiang, H. Shen, D. Chugh, M. Lockrey, D. Zhong, J. Li, K. Weber, T. P. White, K. R. Catchpole, *ACS Energy Lett.* **2018**, 3, 2441.
- [22] X. Yang, G. Wang, D. Liu, Y. Yao, G. Zhou, P. Li, B. Wu, X. Rao, Q. Song, *Curr. Appl. Phys.* **2018**, 18, 1095.
- [23] C. Liu, D. Zhang, Z. Li, X. Zhang, L. Shen, W. Guo, *Adv. Funct. Mater.* **2018**, 28, 1803126.
- [24] R. Chen, T. Bu, J. Li, W. Li, P. Zhou, X. Liu, Z. Ku, J. Zhong, Y. Peng, F. Huang, Y.-B. Cheng, Z. Fu, *ChemSusChem* **2018**, 11, 1467.
- [25] J. Drechsel, M. Pfeiffer, X. Zhou, A. Nollau, K. Leo, *Synth. Met.* **2002**, 127, 201.
- [26] X. Zhou, M. Pfeiffer, J. S. Huang, J. Blochwitz-Nimoth, D. S. Qin, A. Werner, J. Drechsel, B. Maennig, K. Leo, *Appl. Phys. Lett.* **2002**, 81, 922.
- [27] N. Senthilkumar, S. Park, H.-S. Kang, D. W. Park, Y. Choe, *J. Ind. Eng. Chem.* **2011**, 17, 799.
- [28] P. Pahner, H. Kleemann, L. Burtone, M. L. Tietze, J. Fischer, K. Leo, B. Lüssem, *Phys. Rev. B* **2013**, 88, 195205.
- [29] E.-M. Han, L.-M. Do, M. Fujihira, H. Inada, Y. Shirota, *J. Appl. Phys.* **1996**, 80, 3297.
- [30] K. Onlao, B. Tunhoo, P. Keeratithiwakorn, T. Thiwawong, J. Nukeaw, *Solid-State Electron.* **2012**, 72, 60.
- [31] Y.-C. Chiu, B.-H. Chen, D.-J. Jan, S.-J. Tang, K.-C. Chiu, *Cryst. Res. Technol.* **2011**, 46, 295.
- [32] R. Ruiz, D. Choudhary, B. Nickel, T. Toccoli, K.-C. Chang, A. C. Mayer, P. Clancy, J. M. Blakely, R. L. Headrick, S. Iannotta, G. G. Malliaras, *Chem. Mater.* **2004**, 16, 4497.
- [33] O. J. Sandberg, J. Kurpiers, M. Stolterfoht, D. Neher, P. Meredith, S. Shoaee, A. Armin, *Adv. Mater. Interfaces* **2020**, 7, 2000041.
- [34] X. Liu, Y. Wang, F. Xie, X. Yang, L. Han, *ACS Energy Lett.* **2018**, 3, 1116.
- [35] X. Liu, T. Wu, C. Zhang, Y. Zhang, H. Segawa, L. Han, *Adv. Funct. Mater.* **2021**, 31, 2106560.
- [36] A. M. Boehm, T. Liu, S. M. Park, A. Abtahi, K. R. Graham, *ACS Appl. Mater. Interfaces* **2020**, 12, 5209.
- [37] S. T. Birkhold, J. T. Precht, R. Giridharagopal, G. E. Eperon, L. Schmidt-Mende, D. S. Ginger, *J. Phys. Chem. C* **2018**, 122, 12633.
- [38] S. A. L. Weber, I. M. Hermes, S.-H. Turren-Cruz, C. Gort, V. W. Bergmann, L. Gilson, A. Hagfeldt, M. Graetzel, W. Tress, R. Berger, *Energy Environ. Sci.* **2018**, 11, 2404.
- [39] S. Tao, I. Schmidt, G. Brocks, J. Jiang, I. Tranca, K. Meerholz, S. Olthof, *Nat. Commun.* **2019**, 10, 2560.
- [40] C. C. Stoumpos, C. D. Malliakas, M. G. Kanatzidis, *Inorg. Chem.* **2013**, 52, 9019.
- [41] J.-F. Li, S.-F. Chen, S.-H. Su, K.-S. Hwang, M. Yokoyama, *Appl. Surf. Sci.* **2006**, 253, 2522.
- [42] L. Grządziel, J. Żak, J. Szuber, *Thin Solid Films* **2003**, 436, 70.
- [43] J. E. S. Kim, E. Lim, K. Lee, D. Cha, B. Friedman, *Appl. Surf. Sci.* **2003**, 205, 274.
- [44] C. D. Dimitrakopoulos, A. R. Brown, A. Pomp, *J. Appl. Phys.* **1996**, 80, 2501.
- [45] R. Ruiz, B. Nickel, N. Koch, L. C. Feldman, R. F. Haglund, A. Kahn, G. Scoles, *Phys. Rev. B* **2003**, 67, 125406.
- [46] X. Yu, J. Yu, J. Zhou, J. Huang, Y. Jiang, *Appl. Phys. Lett.* **2011**, 99, 63306.
- [47] J. Zhang, J. Wang, H. Wang, D. Yan, *Appl. Phys. Lett.* **2004**, 84, 142.
- [48] B. Jaeckel, J. B. Sambur, B. A. Parkinson, *J. Appl. Phys.* **2008**, 103, 63719.
- [49] P. Zhang, S. Zhao, H. Wang, J. Zhang, J. Shi, H. Wang, D. Yan, *Adv. Electron. Mater.* **2017**, 3, 1700136.
- [50] S. Chen, T. W. Goh, D. Sabba, J. Chua, N. Mathews, C. H. A. Huan, T. C. Sum, *APL Mater.* **2014**, 2, 81512.
- [51] I. G. Hill, A. Kahn, *J. Appl. Phys.* **1999**, 86, 4515.
- [52] S. Braun, W. Osikowicz, Y. Wang, W. R. Salaneck, *Org. Electron.* **2007**, 8, 14.
- [53] S. Braun, M. P. de Jong, W. Osikowicz, W. R. Salaneck, *Appl. Phys. Lett.* **2007**, 91, 202108.
- [54] G. Chauhan, R. Srivastava, P. Tyagi, A. Kumar, P. C. Srivastava, M. N. Kamalasanan, *Synth. Met.* **2010**, 160, 1422.
- [55] R. D. Gould, *Thin Solid Films* **1985**, 125, 63.
- [56] C. H. Kim, O. Yaghmazadeh, D. Tondelier, Y. B. Jeong, Y. Bonnassieux, G. Horowitz, *J. Appl. Phys.* **2011**, 109, 83710.
- [57] J. P. Colinge, C. A. Colinge, *Physics of Semiconductor Devices*, Kluwer Academic Publishers, Boston, MA **2002**.
- [58] Z. Zhang, J. T. Yates, *Chem. Rev.* **2012**, 112, 5520.
- [59] Z. Wan, H. Lai, S. Ren, R. He, Y. Jiang, J. Luo, Q. Chen, X. Hao, Y. Wang, J. Zhang, L. Wu, D. Zhao, *J. Energy Chem.* **2021**, 57, 147.
- [60] J. Hwang, A. Wan, A. Kahn, *Mater. Sci. Eng. R Rep.* **2009**, 64, 1.
- [61] I. G. Hill, A. Rajagopal, A. Kahn, Y. Hu, *Appl. Phys. Lett.* **1998**, 73, 662.
- [62] H. Ishii, N. Hayashi, E. Ito, Y. Washizu, K. Sugi, Y. Kimura, M. Niwano, Y. Ouchi, K. Seki, *Phys. Status Solidi A* **2004**, 201, 1075.
- [63] L. Canil, T. Cramer, B. Fraboni, D. Ricciarelli, D. Meggiolaro, A. Singh, M. Liu, M. Rusu, C. M. Wolff, N. Phung, Q. Wang, D. Neher, T. Unold, P. Vivo, A. Gagliardi, F. de Angelis, A. Abate, *Energy Environ. Sci.* **2021**, 14, 1429.
- [64] W. Xing, S. Wu, Y. Liang, Y. Sun, Y. Zou, L. Liu, W. Xu, D. Zhu, *ACS Appl. Mater. Interfaces* **2020**, 12, 29540.
- [65] J. Horn, M. Scholz, K. Oum, T. Lenzer, D. Schlettwein, *APL Mater.* **2019**, 7, 31112.
- [66] T. Zhang, X. Meng, Y. Bai, S. Xiao, C. Hu, Y. Yang, H. Chen, S. Yang, *J. Mater. Chem. A* **2017**, 5, 1103.
- [67] Y. Yamamoto, K. Yoshino, Y. Inuishi, *J. Phys. Soc. Jpn.* **1979**, 47, 1887.
- [68] M. Brinkmann, V. S. Videva, A. Bieber, J. J. André, P. Turek, L. Zuppiroli, P. Bugnon, M. Schaer, F. Nuesch, R. Humphry-Baker, *J. Phys. Chem. A* **2004**, 108, 8170.
- [69] R. A. Kerner, S. Heo, K. Roh, K. MacMillan, B. W. Larson, B. P. Rand, *ACS Energy Lett.* **2021**, 6, 501.
- [70] V. Arivazhagan, P. Hang, M. M. Parvathi, Z. Tang, A. Khan, D. Yang, X. Yu, *Nanotechnology* **2020**, 31, 65401.
- [71] P. A. Fernández Garrillo, B. Grévin, N. Chevalier, Ł. Borowik, *Rev. Sci. Instrum.* **2018**, 89, 43702.
- [72] S. J. Sque, R. Jones, P. R. Briddon, *Phys. Status Solidi A* **2007**, 204, 3078.
- [73] U. Zerweck, C. Loppacher, T. Otto, S. Grafström, L. M. Eng, *Phys. Rev. B* **2005**, 71, 125424.